Nuclear Engineering and Technology 56 (2024) 3536–3544

Contents lists available at ScienceDirect

Nuclear Engineering and Technology

journal homepage: www.elsevier.com/locate/net

Original Article

Conceptual RF design of 750 MHz IH cavities for $\beta = 0.10$–0.15 ion beams in medical accelerators

Jorge Giner Navarro [a,*], Gabriela Moreno [a], Daniel Gavela [a], Concepción Oliver [a], Pedro Calvo [a], Miguel León [a], Ángel Rodríguez [a], Ricardo López [a], José Miguel Carmona [b], María Alvarado [b]

[a] Department of Technology, CIEMAT, Avenida Complutense 40, Madrid, 28040, Spain
[b] Added Value Industrial Engineering Solutions, Xixilion Kalea 2, Elgoibar, 20870, Spain

ARTICLE INFO

Keywords:
Accelerator
Linac
Interdigital H-mode
DTL
Low-beta
Efficiency

ABSTRACT

In light of the potential interest of Interdigital H-mode (IH) cavities for accelerating carbon ion beams beyond 5 MeV/u, we are reviewing the key geometric elements of the regular cells and end cells to optimize performance in terms of power efficiency, achievable voltage, and dipole field correction.

1. Introduction

In the last decade, several countries have shown interest in equipping their healthcare infrastructure with accelerator systems for cancer therapy through hadron irradiation. Certainly, hadron therapy provides greater precision in tumor irradiation, reducing damage to surrounding healthy tissue and improving the quality of life for patients. Specifically, the use of heavier ions such as carbon ions offers more promising performance against radioresistant tumors than proton therapy techniques, which are currently experiencing a significant increase in adoption. In the accelerators of these facilities, typically based on synchrotrons but also with current developments in cyclotrons, the beam characteristics and irradiation performance are largely determined by the injector.

Injectors represent a key section of any proton or ion beam accelerator complex, as they are the starting segment where beam particles are produced and arranged for the main system. That can be either a synchrotron [1], another linac [2], or even a cyclotron [3]. The first RF component of this section is always the Radiofrequency Quadrupole (RFQ) to initiate the temporal structure of the beam. Considering that a great part of the RF power that feeds the RFQ is used to confine the beam along, the use of more efficient RF structures for acceleration becomes necessary once the appropriate time structure is achieved. It has already been studied that H-mode resonant cavities [4,5] are well-suited to cover an accelerating segment between long-established RFQ and high-β structures. Particularly, Interdigital H-mode Drift Tube Linacs (IH-DTL) offer excellent performance for ion velocities below 15% of the speed of light [6].

One easily finds in the literature accelerator facilities for various applications that use IH-DTL structures, which are particularly employed in the injection of heavy ion beams [7–13]. As regards hadrontherapy linacs, IH cavities are more commonly operated for carbon ion beams rather than protons. Two layouts, based on different approaches to work out the beam dynamics, are used in existing facilities. The first one can be found in Japanese facilities such as NIRS-HIMAC, GHMC, SAGA-HIMAT, and i-ROCK [14,15], and it is based on "Alternating-Phase Focusing" (APF) dynamics configuration. The second one, based on the "Combined Zero-Degree Structure" (KONUS) design, has been the reference design for the injectors at HIT, CNAO, SPHIC, MIT and MedAustron [16]. Both KONUS and APF solutions are consolidated in linear injectors where maximum transmission of high-current beams is required.

The pursuit of compactness in these accelerators has always been a clear motivation towards more cost-effective manufacturing and a reduction in the footprint of the installation, making it feasible to be implemented near densely populated urban areas, where hadron therapy services are meant to be exploited. It is well-known that the use of high RF frequencies aims in this direction, while also seeking to enhance the efficiency of their electrical consumption with a commitment to

* Corresponding author.
E-mail address: jorge.giner@ciemat.es (J. Giner Navarro).

https://doi.org/10.1016/j.net.2024.04.001
Received 9 October 2023; Received in revised form 13 February 2024; Accepted 2 April 2024
Available online 9 April 2024

sustainability. The resonance frequency of existing IH-DTLs, to this date, is of the order of 200–217 MHz, corresponding to a cavity diameter size of 400 mm. A recent design for the XiPAF proton medical facility, working at 325 MHz, demonstrated a reduction of the cavity diameter to 216 mm [17,18]. However, an extremely compact design was proposed at 750 MHz by TERA Foundation and CERN as part of TULIP and CABOTO linac projects [6], for proton and carbon ion beams respectively, with a cavity size starting at only 120 mm.

The progress discussed here on an optimized IH-DTL structure design is part of a national collaboration between industrial companies and research centers aimed at optimizing the early acceleration phase of a carbon ion accelerator for hadron therapy, either to be integrated into the injector of future synchrotrons or as the initial segment of an all-linac facility. The collaboration also includes, among other studies, the development of electron gun prototypes for a C^{6+} ion EBIS source [19] and the manufacturing of the recently designed high-frequency RFQ at CERN [20], which is expected to provide ion energies of up to 5 MeV per nucleon. The initial portion of the RFQ, which would reach 2.5 MeV/u, is scheduled to complete its production and undergo commissioning at CERN premises in 2024 [21]. The work we are concerned with aims to extend the beamline to reach 10 MeV per nucleon using compact IH-DTL cavities operating at 750 MHz. This frequency is particularly convenient to be matched between the 750 MHz RFQ and a future extension with well-established Side-Coupled DTLs (SCDTL) at 3 GHz [22] that boost the energy beyond 10 MeV/u.

Driven by the goal of optimizing the IH geometry, this research

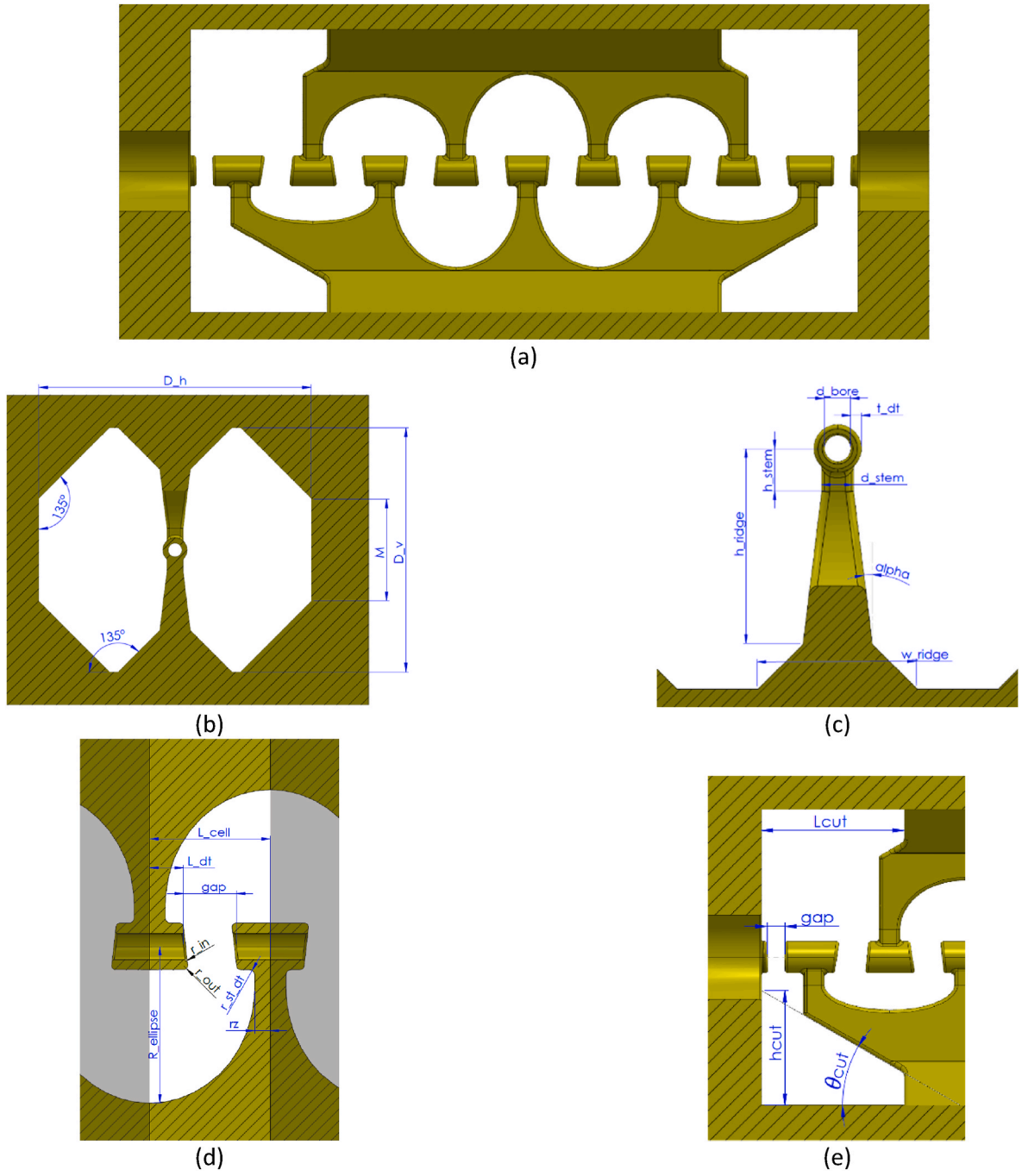

Fig. 1. Section view of a 10-cell IH model (a), provided as an example to detail the dimensional parameters of the regular cells (b–d) and the end cells with undercut (e).

focuses on electromagnetic simulations that enable the characterization of the dimensions for this specific frequency and provide essential reference properties for a comprehensive beam dynamics design. The article is outlined as follows. In Section 2, we will describe all the components that make up the geometry of a regular cell of the RF cavity and highlight the relevant parameters for optimization. The efficiency optimization study over the auto-inductive region of the cell will be described in Section 3, and the characterization of the field limits in the capacitive gap between drift tubes will be analyzed in Section 4. In Section 5, several proposals for geometry modifications will be presented to correct the dipole kick field across the gap. We will also dedicate an analysis, in Section 6, to optimization possibilities focused on the ends of the IH cavities. Lastly, Section 7 will summarize the conclusions and future plans.

2. The RF cell

The simulated models in this study can be applied to other IH-type structures with similar resonance frequencies, designed to accelerate charged particles at speeds between 10 and 15% of the speed of light, as determined by the length of their cells. In the specific case under consideration, the analysis is designed for C^{6+} ion beams with energies ranging from 5 to 10 MeV/u, currents on the order of 0.2 mA in 5-μs pulses, and a repetition rate of 200 Hz. The expected beam from the ion source and the RFQ in the immediately previous stage has a normalized transverse emittance (r.m.s.) below 0.030 π mm·mrad and an r.m.s. transverse beam size around 0.22 mm in both directions [20,21]. Fig. 1 displays various section views of a compact IH-DTL cavity example designed to operate in the $H_{11(0)}$ mode at 750 MHz. The RF simulations carried out in the first part of this article were made considering a single, regular, $\beta\lambda$/2-long cell and applying cell-to-cell "perfect-H" boundary conditions, which means forcing the continuity of the tangential component of the magnetic field. Commercial software, CST Microwave Studio [23], was used for the evaluation of eigenmode electromagnetic fields.

An example of one regular cell, as it is simulated in electromagnetic solvers, is depicted in Fig. 1(b–d). The model is inspired by that proposed in Ref. [6]. The cavity outer profile is defined by flat walls, motivated by the same reasons for machining simplicity as adopted for the 750 MHz RFQ [20]. The preference for reshaping to round walls for the sake of greater efficiency will be discussed in the following section. The horizontal and vertical sizes of the cavity are named D_h and D_v, respectively. The four corners of the cavity are made of 45-degree cuts, which define the M dimension allowing for the space foreseen for RF auxiliaries. The geometries of the stems and drift tubes are also parameterized by several dimensions noted in Fig. 1. Given the large number of parameters, selecting the optimal set of dimensions is a complex task. Regarding the drift tubes, a narrow aperture of 5 mm is adopted, according to the beam dynamics studies of the previous acceleration stage. The wall thickness is set at 2 mm, in agreement with an ultra-precision machining capabilities with tolerances of ±0.05 mm, a common value in analogous cavities [13,18]. This parameter, critical for thermal deformations under high-power conditions, has been previously verified, according to the low duty cycle of the structure [24]. This compact arrangement guarantees favorable shunt impedance while upholding efficient transmission of ion beams within the structure. The tubes are held by a 6 mm-sized connection to the stems, and the junction between adjacent stems is made through elliptical arcs. The remaining parameters have been investigated in the subsequent sections, with a particular focus on two distinct regions. One pertains to the outer cavity profile, which impacts the auto-inductive regime and involves the magnetic field and RF currents through the walls. The second region refers to the capacitance between drift tubes and involves the electric field for acceleration.

3. Efficiency in auto-inductive region

On metallic surfaces that are not perfect conductors, the electromagnetic fields penetrate the material to a certain depth, resulting in a dissipated power density within the walls:

$$\frac{dP}{dA} = \frac{1}{2} R_s H_s^2 \tag{1}$$

where R_s is the surface resistance of the cavity (7.1 m Ω for copper at 750 MHz), and H_s is the magnetic field on the surface, which can be considered uniform on the cavity profile at first-order approximation. Equation (1) reveals that one would need to reduce the area of the copper walls enclosing the cavity to reduce the dissipated power in the cell. This is confirmed in simulations for different profiles parameterized by D_v, D_h and M (see Fig. 2). The RF power losses increase at a rate of 0.13 W per additional mm^2 of copper surface at a nominal effective voltage of 120 kV and, consequently, the effective shunt impedance ZTT decreases. Generally, there is an increment of ZTT when reducing the vertical size D_v of the cavity, but this must be compensated horizontally with wider D_h in order to retune the resonance.

The reduction of D_v is limited at a certain level by other parameterized dimensions of the stems, such as $R_{ellipse}$, as it is obvious that the cavity size cannot be smaller than the stem size. In Fig. 3(a), the variation of ZTT was evaluated for different proportions of D_v and $R_{ellipse}$. This could not be assessed for values of D_v below the mentioned limit and, for this reason, the trend of increasing ZTT is cut. It is found optimal to maximize $R_{ellipse}$ so that the ellipse edge which describes the stem shape ends on the corresponding ridge. That is:

$$R_{ellipse}^{opt} = h_{ridge} - r_{st} \tag{2}$$

where r_{st} is the small rounding of 1.5 mm at the ridge edge. As one can note in Fig. 1(d), the optimum dimension of $R_{ellipse}$ agrees with the minimum possible surface area of copper of the vane-stem that produces the H field in the auto-inductive region.

We find the size of the lateral wall, indicated by the M dimension, to be critical for the optimization. This flat wall, for both left and right sides, is intended to allocate power couplers, vacuum ports and tuners, thus a minimum width of 38 mm will be required as it was designed for the RFQ [20]. In Fig. 3(b), the effective shunt impedance is analyzed as a function of M, and establishing the optimal $R_{ellipse}^{opt}$ in each case. ZTT is consistently larger as the lateral wall width shrinks. For this reason, it is found convenient to restrict the M dimension to its minimum possible value of 38 mm.

Based on the same principle of area reduction to improve ZTT, we studied the effect on rounding the walls of the outer profile of the cavity,

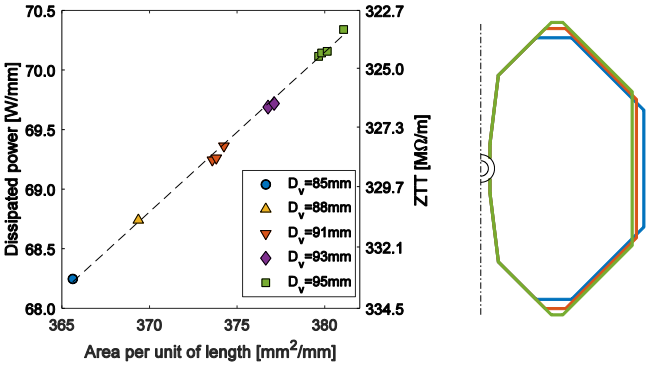

Fig. 2. Relation between dissipated power and copper surface area per unit of cell length (left), extracted from single-cell simulations with different profiles at a fixed resonant frequency (750 MHz). Power is scaled to a corresponding effective gap voltage of 120 kV. Three selected profiles of the auto-inductive region are represented (right).

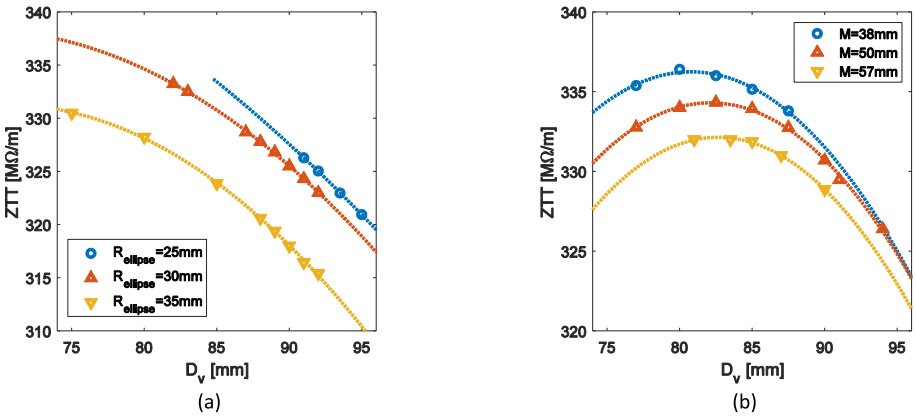

Fig. 3. Shunt impedance as a function of cavity size D_v for different values of (a) $R_{ellipse}$ and (b) M.

yet still leaving two 38 mm-wide, flat walls at both laterals reserved for RF auxiliaries. Two new rounded models are shown in Fig. 4(b and c) for a single, 25.16 mm-long cell, compared to the one with flat walls. The first one maintains the ridge at the base of the stems, and the second does not have a ridge. The dimensions of the stems are the same in all cases in order to make a suitable comparison of the effect of the outer profile, although the horizontal size of the cavity D_h has been adjusted to tune the cavity at the same resonant frequency. Alternative geometries with round profiles were also explored in a previous study [25].

The effective shunt impedance results are presented in Table 1. On one hand, a noticeable decrease in shunt impedance is observed if the ridge is removed. On the other hand, maintaining the same ridge results in a marginal increase when rounding the walls. However, this efficiency enhancement is insufficient, and the option with flat walls is favored due to considerations of machinability.

4. Field limits in capacitive-gap region

In this section, we explore the capacitive-dominated region of the IH cell. That is the space between drift tubes with opposed charges that generates the voltage for the beam acceleration. The electric field profile across the gap on the centered axis is represented in Fig. 5. If the cavity size (D_v or D_h) is altered but the shape and dimensions of the drift tubes remain fixed, we verify that the resonant frequency moves but the electric field is practically unchanged. The gap size determines the capacitance across the drift tubes; thus, shorter gaps are related to smaller resonant frequencies than larger ones. For this reason, we can consider that the influence on the beam dynamics is much stronger by the dimensions of the gap and drift tubes rather than the frequency tuning of the whole cell.

As the gap size increases, the transit time factor drops following, in good approximation, the typical trend of a sine-cardinal function [26].

Table 1
Shunt impedance and horizontal size of three outer profiles under study. In all cases, the cell length is 25.16 mm and vertical size is 90 mm.

	D_h [mm]	ZTT [M Ω/m]
Flat walls	104.74	330.63
Round walls with ridge	97.02	331.71
Round walls without ridge	96.78	324.16

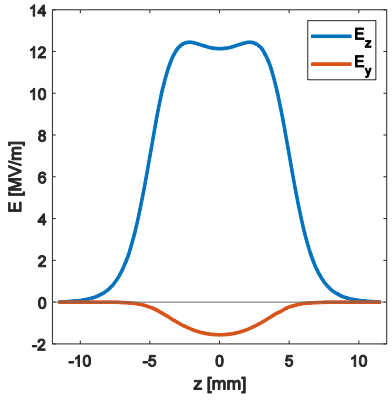

Fig. 5. Axial and transverse field on the centered axis of a standard 23.085 mm IH cell.

Limited by the minimum length of each drift tube that is supported by the stem, it is evident that the gap size can be wider for longer cells. This allows for achieving greater voltages across the gap if the same average gradient is conserved since it implies that a smaller accumulation of

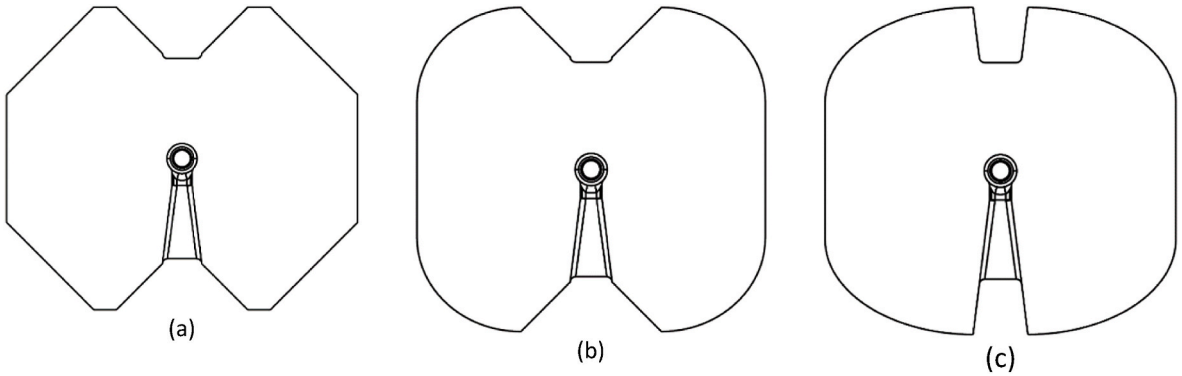

Fig. 4. Models with (a) flat walls, and round walls (b) with a ridge, and (c) without a ridge at the outer profile of the cavity.

electric field is produced in the vicinities of the drift tubes. The voltage restriction, at 750 MHz, is given by Kilpatrick's field limit on the copper surface due to vacuum arcs [27], corrected above by an acceptable but safe bravery factor of 2, and it is set by design to a maximum field of 50.6 MV/m.

Simulations have been performed in CST for different cell lengths and gap sizes. Maximum effective voltages, including transit time factor, have been evaluated under surface field considerations and shown in Fig. 6(a). In general, this voltage reaches a steady plateau for gaps that use above 40% of the cell's total length. The shortest cells, corresponding to carbon ion speeds of $\beta \simeq 0.10$ (5 MeV/u), can drive up to 126 kV, while the longest cells, for $\beta \simeq 0.15$ (10 MeV/u), up to 149 kV.

A refinement of the drift tube shape grants a smaller peak field, thereby allowing for a greater voltage. For instance, a wider rounding of the drift tube edges is needed to soften the electric field on the copper. Fig. 6(b) shows how the voltage limit can be increased by making the rounding of the outer edge r_{out} larger, while the rounding of the inner edge r_{in} is not relevant.

5. Dipole electric field correction

Structures with very small apertures, and high-frequency regimes, require special attention to the beam dynamics, which is strongly affected by small errors in geometry dimensions. In addition, the asymmetry with opposing stems introduces a very significant transverse component of the electric field. Benedetti et al. [6] proposed the mitigation of such dipole kick by adjusting the length of the first and last cells of the RF tank. In this study, we consider several proposals for geometrical modifications of the drift tubes that aim at either reducing or compensating the transverse electric fields. Simulations of the electromagnetic fields were performed in CST [23], and calculations of different figures of merit were compared for each model.

We recall Fig. 5, which represents the axial (z) and transverse (y) components of the electric field along the ideal particle path through a single-cell model of 23.085 mm, corresponding to an ion speed of $\beta = 0.12$. The transverse voltage, responsible for deflecting the beam, entails 8.4% of the total axial voltage in a single cell. The goal of this study is to reduce the deflecting effect by modifying the standard drift tube geometry close to the gap.

Four variations of the drift tubes are analyzed in this study, as shown in Fig. 7. For the sake of a fair comparison, the gap and the stem dimensions are the same as in the standard cell. One dimension of the new feature is used as an optimization parameter to minimize the transverse deflection.

A common choice of dipole correction is adding small bulges at the edges of the drift tube [4,10] that compensate for the electric field orientation from the accumulated charge in the stems. This bulge, shown in Fig. 7(a)–is modeled as a 2 mm thick circular disk, with a larger diameter than the drift tube, but off-centered, so that it makes a tangent point on the side of the connection with the stem bar. Based on the same principle as the circular disk, a racetrack shape is adopted to reduce the bulging material on the laterals of the drift tube. As it can be seen in Fig. 7(b), one arc of the racetrack is matched to the drift tube contour, and the center of the second arc is displaced by an offset.

For the third variation, instead of machining bulges, the whole drift tube is designed so that the aperture where the beam travels is off-center. In our model, shown in Fig. 7(c), we keep the aperture and the stem connection in the same position as the standard cell, but we introduce an offset for the cylinder axis that defines the copper-made drift tube.

The last variation introduces a slant in opposing faces at the edges of the drift tubes [5], as depicted in Fig. 7(d). In this way, we intend to compensate for the asymmetry of the inverted stems and reorient the electric field lines across the gap.

The dipole correction strategy consists of finding the zero of the integral of the transverse field component normalized to the axial voltage:

$$\frac{V_y}{V_z} = \frac{\int E_y(z)\,\mathrm{d}z}{\int E_z(z)\,\mathrm{d}z} \tag{3}$$

For circular and racetrack features, the disk height is used as the optimization parameter; for the off-centered aperture approach, we use the drift tube height; and for the slant faces, we optimize the angle of opposing faces with respect to the original. The results of V_y/V_z as a function of the optimization parameter are represented for all drift tube variations in Fig. 8. One finds monotonous trends where zero-crossing separates between positive (the field is oriented upwards) and negative (downwards) deflection. Since the new shape changes the capacitance between tubes, the resonant frequency is shifted by a few MHz. This is tuned back to the nominal value (750 MHz) by adjusting the size of the outer profile of the cavity, which only affects the auto-inductive region.

The electric fields on the beam axis have been evaluated for the optimized variations (Fig. 9). The geometries with bulges and with off-center apertures achieve very low levels of transverse field across the gap, offering a fairly uniform profile with ripples of about 100 kV/m. Contrastingly, the field profile produced by the slanted faces variation shows three peaks of alternating field direction in the y-axis, although the net voltage due to the transverse field is still zero. It is noted that the maximum peak is half of the standard one.

The effect of the field shape caused by the angled faces variation is simulated for a single C^{6+} ion entering the cell on a centered axis with no angle, and a velocity of $\beta = 0.12$, by solving $\mathrm{d}\vec{p}/\mathrm{d}t = q\vec{E}$. The ion trajectory, depicted in Fig. 10, describes a very small deflection at its halfway point and gets corrected at the exit back to zero offset position

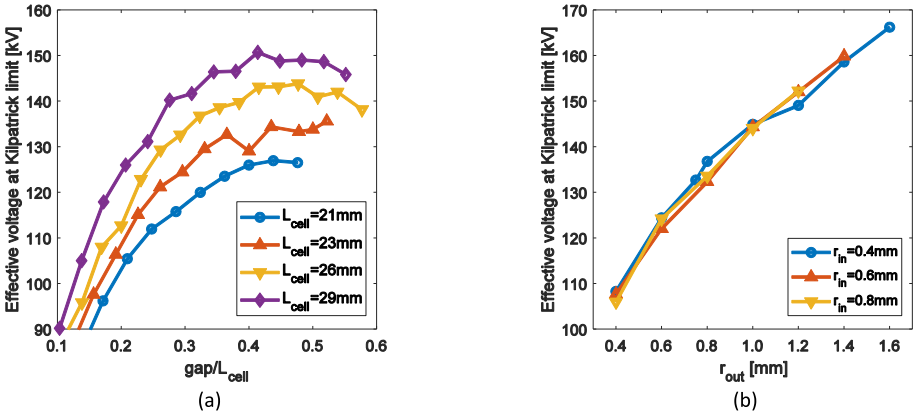

Fig. 6. Maximum voltage across the gap that can be achieved for (a) different cell lengths and gap sizes of an IH cell, and (b) different roundings of drift tube edges in an IH cell length of 23 mm and gap size of 9.2 mm, considering a maximum surface electric field of 50.6 MV/m.

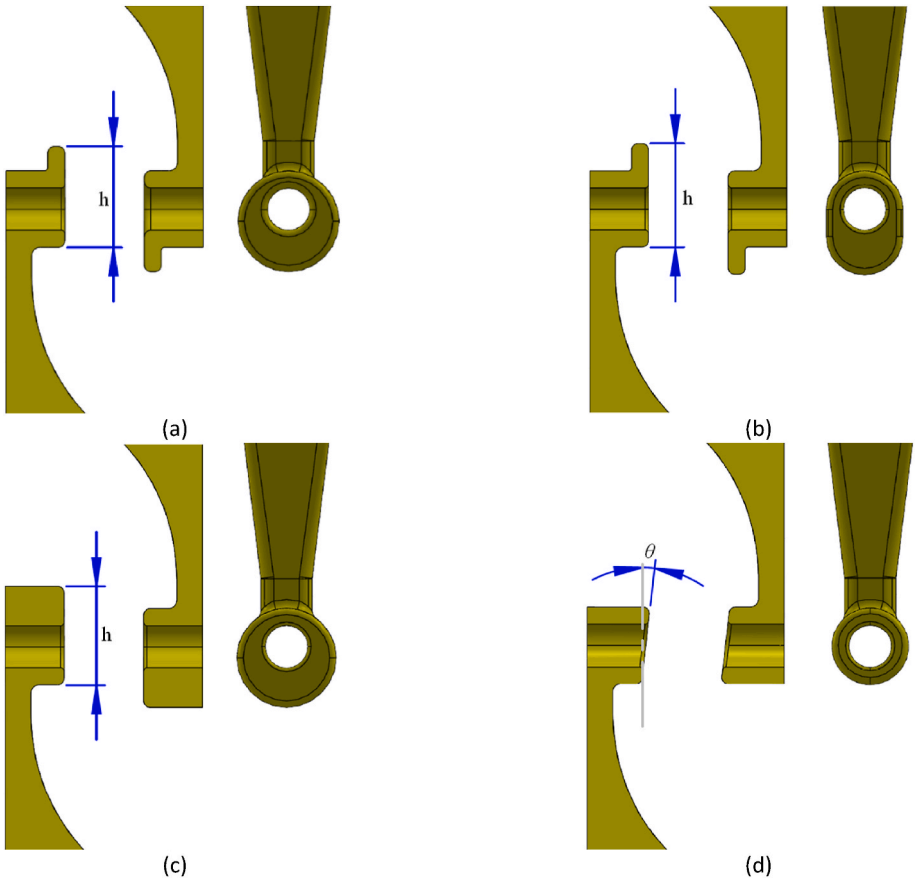

Fig. 7. Four proposals of drift tube modifications for electric dipole compensation: (a) circular disk, (b) racetrack disk, (c) off-centered aperture and (d) slant faces.

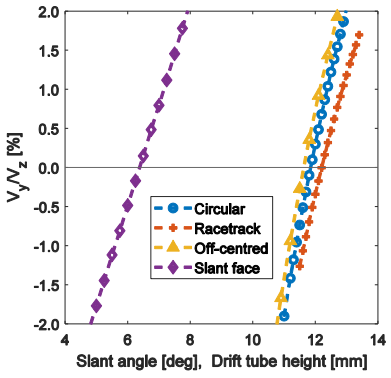

Fig. 8. Optimization curves of four variations for V_y/V_z minimisation.

and angle, which is the optimum for entering the following cell.

To compare the performance and suitability of each variation that suppresses the electric dipole component, we analyze in Table 2 a series of figures of merit.

The size of the cavity (D_v and D_h) is adjusted to tune the resonant frequency to 750 MHz. Adding more material to the drift tubes, as is the case for the first three variants, increases the electric capacitance and decreases frequency. For this reason, the size of the cavity needs to be from 6 to 9 mm smaller. When only introducing a small slant on drift tube faces, electric capacitance is barely altered. The transit time factor (T) is nearly identical for all cases, which is mainly dominated by the gap size.

We do find a large diversity in the results of the effective shunt impedance, a relevant indicator of the power efficiency performance of the RF cavity. The circular disk feature degrades efficiency by 25% while removing lateral material with a racetrack shape achieves a little less degradation (19%). The worst performance is given by the off-centered aperture version, which loses 30% of shunt impedance. The slant faces variation represents the least modification of the geometry, thus the smallest degradation of ZTT is accomplished (1%). This performance makes the latter a promising candidate to be applied to a full IH structure.

The field enhancement factor (η) is defined here as the ratio between the peak electric field on the copper surface and the average on-axis gradient. Most of the models show an increase in the peak surface field. Aiming at the maximum surface field of 50.6 MV/m, the proposed variations allow for a maximum effective axial voltage (V_zT) above 136 kV. The nominal voltage in design for the 23.085 mm long cell presented here is 120 kV, still below the potential breakdown limits on dipole-corrected models.

6. End cells

In pursuit of a complete RF design for a 750 MHz IH-DTL, the end cells of the structure are analyzed and optimized differently from the periodicity of the individual cells. To ensure the magnetic field lines of the H_{11} dipole mode close upon themselves, transitioning to E-mode, a cut is made on the ridges holding the stems at both ends [4]. This feature, denominated undercut, has a negative impact on the overall RF power loss in the cavity. Over the undercut surface, there is a higher concentration of magnetic field lines and currents, leading to increased power dissipation density. In addition, the voltage across the end gap is smaller than in the other gaps, therefore the overall shunt impedance of the structure is certainly degraded.

Fig. 1(e) shows the model used for simulating the RF fields in CST

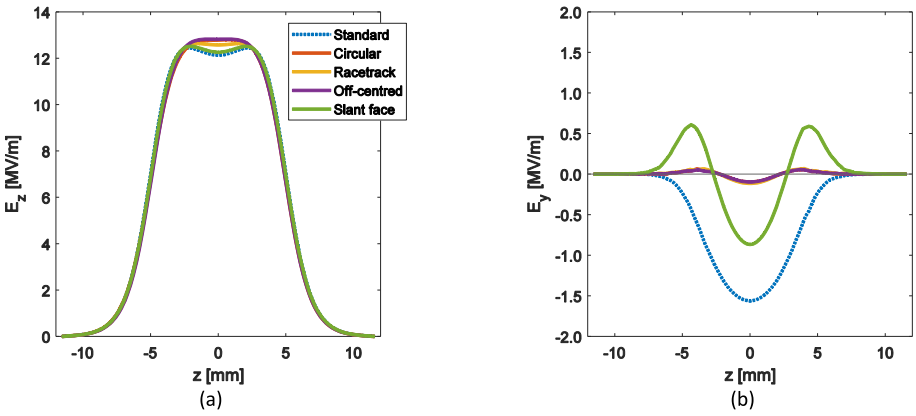

Fig. 9. Axial (a) and transverse (b) electric field profile for the standard cell and presented four variations. Fields are scaled to an axial effective voltage of 120 kV.

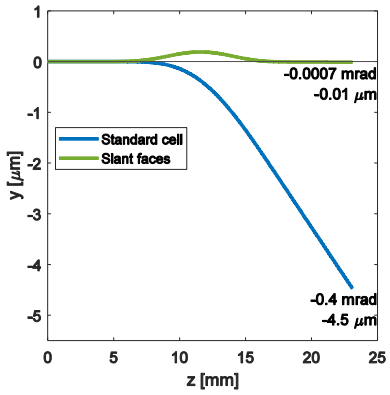

Fig. 10. Particle trajectory comparison between the standard cell and the angled faces variation, for an effective axial voltage of 120 kV.

Table 2
Figures of merit on standard cell and variations.

Model	D_v, D_h [mm]	T	ZTT [M Ω/m]	η	$(V_zT)_{max}$ [kV]
Standard	91.1	0.902	361	7.8	149
Circular disk	83.6	0.907	271	8.1	143
Racetrack disk	85.2	0.905	291	8.6	136
Aperture off-centre	82.3	0.907	257	7.4	158
Slant faces	90.8	0.903	358	8.4	140

Studio at the end of the cavity. It consists of three gaps, in which two of the cells, namely #1 and #2, have a regular geometry as described so far. The end cell, referred to as #0, comprises a conducting lid wall, half of a drift tube attached to it, and the opposing half stem of the adjacent cell. Two trapezoidal undercuts are modeled with proper roundings of the edges, whose geometry is parameterized in the figure by their length L_{cut}, their height h_{cut}, and their angle θ_{cut} subtended with respect to the base surface of the ridge. The open face of the third cell is assigned a Perfect-H boundary condition. The elliptical arcs connecting the stems are adjusted to ensure the mechanical feasibility of the end stem held at a certain distance from the ridge. For the next stem, we have removed the final elliptical arc as expected in a regular cell, and it terminates at a vertical wall, as it has been observed to result in lower RF losses due to reduced copper surface [28]. The effective shunt impedance, averaged over the voltages along the three cells and the power dissipated by the whole assembly, drops to 250 M Ω/m, compared to the 375 M Ω/m achieved for a regular cell of the same length. This degradation highlights the desirability of using IH tanks with a large number of cells to mitigate the effect of the ends.

Two approaches have been adopted to study the optimization possibilities. First, we have analyzed, as shown in Fig. 11, the effect on losses of varying the undercut dimensions, but keeping the rest of the cell dimensions fixed. One of the three parameters is chosen to tune the eigenmode frequency at 750 MHz, in this case, the cut length L_{cut}. According to the results, shorter cuts with larger angles are clearly preferred to reduce losses. This behavior is confirmed when we increase the size of the cavity in the vertical direction D_v; the detuning of the resonance is compensated by a shorter undercut, resulting in a higher overall shunt impedance. Widening the cavity only at the ends is a strategy in line with the method proposed in Ref. [29] for side-cell coupling through the ends of H-mode cavities.

Secondly, we have investigated the effect of the end cell #0 length and the end gap size. We see no meaningful effect of the undercut shape on the voltage across the gap of the end cell. Fig. 12 shows the electric field profiles on the z-axis at different cell and gap #0 dimensions. With a 9 mm gap, the effective axial voltage across the end gap is 67 kV, compared to the reference 120 kV in the immediately following cells. Reducing the gap size to just 4 mm produces a greater gradient, but also increases the effective voltage to 11 kV due to the transit-time factor enhancement. Despite this gain, the shunt impedance remains unaffected, as it also results in more losses. And, although the length of the end cell does not affect the voltage, a slight improvement in ZTT can be seen for shorter lengths as it defines less surface for RF currents through the outer profile walls.

7. Conclusions

In pursuit of a highly efficient performance of the introduced 750

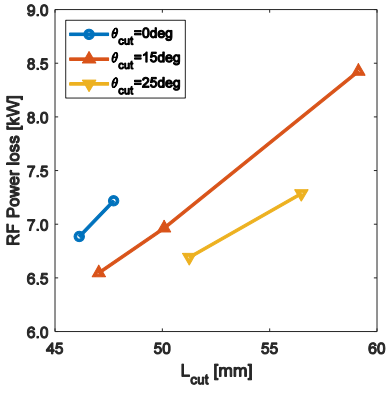

Fig. 11. RF power losses over three simulated end cells at 120 kV effective voltage for the inner cells #1 and #2.

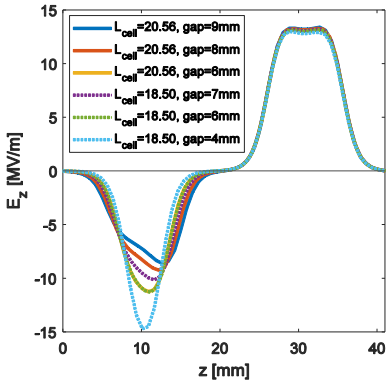

Fig. 12. Longitudinal electric field along the two ending cells on the z-axis at 120 kV effective voltage for the inner cell #1.

MHz IH cavity, an effort has been made here to parameterize most of the dimensions of a single cell, as well as for the undercut features of the end cells. Reducing the area of copper that holds the RF currents is the key to lower power losses, thus we have explored different profiles of the cavity. The approach of rounding the walls of the IH tank is slightly beneficial to electricity consumption costs, however at the expense of a somewhat higher degree of complexity in its fabrication. Nonetheless, the outer profile of the cavity does not require the tightest tolerances, as it does for the drift tubes, since any undesired machining errors are intended to be corrected with external tuning tools. It should also be mentioned that the efficiency enhancement achieved in this study makes no special relevance in the choice of the power source (typically IOTs or solid-state amplifiers), considering that the maximum available power will be safely foreseen to be well above the required input power.

Concerning the gap region of the IH cells, we have a better understanding of the field limits we may encounter during high-power operation as a function of the gap and cell dimensions. Breakdown occurrences are foreseen to be worrisome, especially for the shortest cells of the IH when having voltages above 120 kV. This has been taken into account when introducing geometry modifications for dipole kick correction. Among the proposed variations, the variation with slant faces is a promising feature that will be considered in the future as it shows the lowest impact on machining and power efficiency.

As a result of the findings from this conceptual study, the intention is to produce a first cavity prototype, in a short 16-cell version for 5 MeV/u carbon ions, as a consolidation of the activities of the national collaboration between Spanish industry companies and CIEMAT, funded by the IKERTU project. Achieving this milestone would represent the first-time validation of the feasibility of such a high resonance frequency in these types of cavities, thereby taking advantage of their high power efficiency. The company Added Value Solutions (AVS) is currently undertaking the mechanical design, assembly, alignment, and testing of the cavity, while EGILE will be responsible for the ultra-high precision machining of drift tubes and stems. Preliminary studies of the thermo-mechanical behavior of this structure have already been conducted to estimate the necessary cooling [24]. The dimensions analyzed throughout this manuscript have been taken into account in the mechanical design when assessing the required manufacturing tolerances, with particular attention to those involving the capacitive regions to generate the desired voltage across the gaps. Especially for high-frequency structures, dimensional errors lead not only to a loss of power efficiency compared to the original design but also to an imbalance of voltages along the different cells. Therefore, metrological characterization and tuning of the structure are necessary. The ultimate goal is to conduct prototype commissioning at low power in 2024 using bead-pull measurements on the available testing bench at CIEMAT for tuning and the characterization of gap voltages, quality factor, and shunt impedance. Additionally, the performance of the cavity at high power regimes will also be assessed.

Declaration of competing interest

The authors declare that they have no known competing financial interests or personal relationships that could have appeared to influence the work reported in this paper.

Acknowledgements

The authors would like to thank the financial support for this work by local Basque government through the IKERTU-II project, ZE-2021/00050.

References

[1] M. Vretenar, J. Vollaire, R. Scrivens, C. Rossi, F. Roncarolo, S. Ramberger, U. Raich, B. Puccio, D. Nisbet, R. Mompo, S. Mathot, C. Martin, L.A. Lopez-Hernandez, A. Lombardi, J. Lettry, J.B. Lallement, I. Kozsar, J. Hansen, F. Gerigk, A. Funken, J.F. Fuchs, N. Dos Santos, M. Calviani, M. Buzio, O. Brunner, Y. Body, P. Baudrenghien, J. Bauche, T. Zickler, Linac4 Design Report, CERN, Geneva, 2020, https://doi.org/10.23731/CYRM-2020-006.

[2] D. Ungaro, A. Degiovanni, P. Stabile, LIGHT: a linear accelerator for proton therapy, in: JACOW, Geneva, Switzerland, 2017, pp. 1282–1286, https://doi.org/10.18429/JACoW-NAPAC2016-FRB1IO02.

[3] W. Pelzer, Operation of the RFQ-injector at the ISL cyclotron, Nukleonika 48 (Supplement 2) (2003) S25–S28. http://web.ichtj.waw.pl/www/back/full/vol48_2003/v48s2p025f.pdf.

[4] U. Ratzinger, H-type linac structures. https://doi.org/10.5170/CERN-2005-003.351, 2005.

[5] S.S. Kurennoy, L.J. Rybarcyk, J.F. O'Hara, E.R. Olivas, T.P. Wangler, H -mode accelerating structures with permanent-magnet quadrupole beam focusing, Phys. Rev. Spec. Top. Accel. Beams 15 (2012) 090101, https://doi.org/10.1103/PhysRevSTAB.15.090101.

[6] S. Benedetti, High-gradient and High-Efficiency Linear Accelerators for Hadron Therapy, EPFL, 2018, https://doi.org/10.5075/epfl-thesis-8246.

[7] A.V. Butenko, E.D. Donets, E.E. Donets, V.V. Fimushkin, A. Govorov, A. D. Kovalenko, K.A. Levterov, I.N. Meshkov, V. Monchinsky, A.Y. Ramsdorf, A. O. Sidorin, G.V. Trubnikov, Development of the NICA Injection Facility, JACoW Publishing, Geneva, Switzerland, Shanghai, China, 2013, pp. 3915–3917. https://jacow.org/IPAC2013/papers/THPWO069.pdf.

[8] U. Ratzinger, Commissioning of the new GSI high current linac and HIF related RF linac aspects, Nucl. Instrum. Methods Phys. Res. Sect. Accel. Spectrometers Detect. Assoc. Equip. 464 (2001) 636–645, https://doi.org/10.1016/S0168-9002(01)00155-3.

[9] H. Hähnel, U. Ratzinger, R. Tiede, The KONUS IH-DTL proposal for the GSI UNILAC poststripper linac replacement, J. Phys. Conf. Ser. 874 (2017) 012047, https://doi.org/10.1088/1742-6596/874/1/012047.

[10] J.H. Hähnel, Development of an IH-type linac for the acceleration of high current heavy ion beams, Johann Wolfgang Goethe-Universität in Frankfurt am Main (2017). https://ubffm.hds.hebis.de/Record/HEB415235022.

[11] U. Ratzinger, H. Hähnel, R. Tiede, J. Kaiser, A. Almomani, Combined zero degree structure beam dynamics and applications, Phys. Rev. Accel. Beams 22 (2019) 114801, https://doi.org/10.1103/PhysRevAccelBeams.22.114801.

[12] L. Lu, T. Hattori, N. Hayashizaki, CW operation on APF-IH linac as a heavy ion implanter, Nucl. Instrum. Methods Phys. Res. Sect. Accel. Spectrometers Detect. Assoc. Equip. 622 (2010) 485–491, https://doi.org/10.1016/j.nima.2010.07.043.

[13] L. Zhao, J. Pang, X. He, Z. Ying, J. Shi, Design of an alternating phase focusing Interdigital H-mode Drift-Tube-Linac with low injection energy, Nucl. Instrum. Methods Phys. Res. Sect. Accel. Spectrometers Detect. Assoc. Equip. 806 (2016) 75–79, https://doi.org/10.1016/j.nima.2015.10.007.

[14] Y. Iwata, S. Yamada, T. Murakami, T. Fujimoto, T. Fujisawa, H. Ogawa, N. Miyahara, K. Yamamoto, S. Hojo, Y. Sakamoto, M. Muramatsu, T. Takeuchi, T. Mitsumoto, H. Tsutsui, T. Watanabe, T. Ueda, Alternating-phase-focused IH-DTL for an injector of heavy-ion medical accelerators, Nucl. Instrum. Methods Phys. Res. Sect. Accel. Spectrometers Detect. Assoc. Equip. 569 (2006) 685–696, https://doi.org/10.1016/j.nima.2006.09.057.

[15] K. Yamamoto, H. Tanaka, H. Harada, K. Sugahara, H. Inoue, S. Kawasaki, T. Nagayama, S. Ueda, Experimental verification of an APF linac for a proton therapy facility, Nucl. Instrum. Methods Phys. Res. Sect. B Beam Interact. Mater. Atoms 269 (2011) 2875–2878, https://doi.org/10.1016/j.nimb.2011.04.046.

[16] Y. Lu, Development of an IH-DTL injector for the Heidelberg cancer therapy project, Universitätsbibliothek Johann Christian Senckenberg (2005). http://publikationen.ub.uni-frankfurt.de/frontdoor/index/index/docId/4063.

[17] Y. Lei, X. Guan, C. Tang, R. Tang, X. Wang, Q. Xing, S. Zheng, RF and primary beam dynamics design of a 325 MHz IH-DTL, in: JACOW, Geneva, Switzerland, 2017, pp. 2332–2335, https://doi.org/10.18429/JACoW-IPAC2017-TUPVA104.

[18] P.F. Ma, R. Tang, Y. Yang, S.X. Zheng, W.B. Ye, M.W. Wang, W.L. Liu, B.C. Wang, Q.Z. Xing, C.T. Du, H.Y. Zhang, J. Li, X.L. Guan, X.W. Wang, Z.M. Wang, M.T. Qiu, Development of a compact 325 MHz proton interdigital H -mode drift tube linac

with high shunt impedance, Phys. Rev. Accel. Beams 24 (2021) 020101, https://doi.org/10.1103/PhysRevAccelBeams.24.020101.
[19] R. Mertzig, M. Breitenfeldt, S. Mathot, J. Pitters, A. Shornikov, F. Wenander, A high-compression electron gun for C6+ production: concept, simulations and mechanical design, Nucl. Instrum. Methods Phys. Res. Sect. Accel. Spectrometers Detect. Assoc. Equip. 859 (2017) 102–111, https://doi.org/10.1016/j.nima.2016.12.036.
[20] V. Bencini, H.W. Pommerenke, A. Grudiev, A.M. Lombardi, 750 MHz radio frequency quadrupole with trapezoidal vanes for carbon ion therapy, Phys. Rev. Accel. Beams 23 (2020) 122003, https://doi.org/10.1103/PhysRevAccelBeams.23.122003.
[21] M. Koopmans, D. Gavela, F. Di Lorenzo, A. Lombardi, C. Oliver, E. Pasino, G. Moreno, J. Giner Navarro, J. Perez Morales, P. Calvo, S. Mathot, Preparations for beam commissioning of the carbon RFQ at CERN, in: Proc IPAC23, JACoW Publishing, Geneva, Switzerland, Venice, Italy, 2023, pp. 4961–4964, https://doi.org/10.18429/jacow-ipac2023-thpm057.
[22] C. Ronsivalle, L. Picardi, A. Ampollini, G. Bazzano, F. Marracino, P. Nenzi, C. Snels, V. Surrenti, M. Vadrucci, F. Ambrosini, First acceleration of a proton beam in a side coupled drift tube linac, Europhys. Lett. 111 (2015) 14002, https://doi.org/10.1209/0295-5075/111/14002.
[23] Dassault Systemes, CST Studio suite. https://www.3ds.com/products-services/simulia/products/cst-studio-suite/, 2022.
[24] G. Moreno, J. Giner Navarro, D. Gavela, P. Calvo, M. Leon Lopez, C. Oliver, J. Perez Morales, A. Rodriguez Paramo, J. Carmona, M. Alvarado Martin, A. Lombardi, Thermal and deformation analysis of a 750 MHz IH-DTL prototype for medical applications, in: Proc IPAC23, JACoW Publishing, Geneva, Switzerland, 2023, pp. 1677–1680, https://doi.org/10.18429/jacow-ipac2023-tupa170.
[25] G. Moreno, M.C. Battaglia, P. Calvo, J.M. Carmona, D. Gavela, J. Giner Navarro, A. Lombardi, R. López López, C. Oliver, J. Pérez Morales, Effect of high-magnetic field region geometry on the efficiency of a 750 MHz IH structure, in: JACOW Publishing, Geneva, Switzerland, 2022, pp. 150–153, https://doi.org/10.18429/JACoW-LINAC2022-MOPOGE05.
[26] T.P. Wangler, RF Linear Accelerators, John Wiley & Sons, Ltd, 2008, https://doi.org/10.1002/9783527623426.
[27] W.D. Kilpatrick, Criterion for vacuum sparking designed to include both rf and dc, Rev. Sci. Instrum. 28 (1957) 824–826, https://doi.org/10.1063/1.1715731.
[28] G. Moreno, J. Giner Navarro, D. Gavela, P. Calvo, M. Leon Lopez, C. Oliver, J. Perez Morales, A. Rodriguez Paramo, J. Carmona, M. Alvarado Martin, A. Lombardi, H11 (0) end cells for a 750 MHz IH structure, in: Proc IPAC23, JACoW Publishing, Geneva, Switzerland, 2023, pp. 1681–1684, https://doi.org/10.18429/jacow-ipac2023-tupa171.
[29] U. Amaldi, A. Citterio, M. Crescenti, A. Giuliacci, C. Tronci, R. Zennaro, CLUSTER: a high-frequency H-mode coupled cavity linac for low and medium energies, Nucl. Instrum. Methods Phys. Res. Sect. Accel. Spectrometers Detect. Assoc. Equip. 579 (2007) 924–936, https://doi.org/10.1016/j.nima.2007.05.208.